Structures of Heparin-Derived Disaccharide Bound to Cobra Cardiotoxins: Context-Dependent Conformational Change of Heparin upon Binding to the Rigid Core of the Three-Fingered Toxin†

Shih-Che Sue,‡ Jean-Robert Brisson,§ Siu-Cin Chang,‡ Wei-Ning Huang,‡ Shao-Chen Lee,‡ Harold C. Jarrell,§ and Wen-guey Wu*,‡

Department of Life Sciences, National Tsing Hua University, Hsinchu 30043, Taiwan, and Institute for Biological Sciences, National Research Council, Ottawa K1A 0R6, Canada

Received April 25, 2001; Revised Manuscript Received June 18, 2001

ABSTRACT: Glycosaminoglycans (GAGs) have been suggested to be a potential target for cobra cardiotoxin (CTX) with high affinity and specificity via a cationic belt at the concave surface of the polypeptide. The interaction of GAGs, such as high-molecular weight heparin, with CTXs not only can induce aggregation of CTX molecules but also can enhance their penetration into membranes. The binding of short chain heparin, such as a heparin-derived disaccharide [ΔUA2S(1→4)-α-D-GlcNS6S], to CTX A3 from Taiwan cobra (*Naja atra*), however, will not induce aggregation and was, therefore, investigated by high-resolution ^{1}H NMR. A novel heparin binding site on the convex side of the CTX, near the rigid disulfide bond-tightened core region of Cys38, was identified due to the observation of intermolecular NOEs between the protein and carbohydrate. The derived carbohydrate conformation using complete relaxation and conformational exchange matrix analysis (CORCEMA) of NOEs indicated that the glycosidic linkage conformation and the ring conformation of the unsaturated uronic acid in the bound state depended significantly on the charge context of CTX molecules near the binding site. Specifically, comparative binding studies of several heparin disaccharide homologues with two CTX homologues (CTX Tγ from *Naja nigricolli*s and CTX A3) indicated that the electrostatic interaction of *N*-sulfate of glucosamine with $NH_3^+\zeta$ of Lys12 and of the 2-*O*-sulfate of the unsaturated uronic acid with $NH_3^+\zeta$ of Lys5 played an important role. These results also suggest a model on how the CTX−heparin interaction may regulate heparin-induced aggregation of the toxin via the second heparin binding site.

Cardiotoxins (or cytotoxins, CTXs)[1] from cobra venom are highly basic, slightly curved, all-β-sheet polypeptides capable of inducing general cytotoxic effect on many cell types, including cardiac myocytes (*1*, *2*). They also cause severe tissue necrosis and local gangrene in humans by an unknown mechanism (*3*). To explain the general cytotoxic effect of CTXs with certain cell specificity, we have recently proposed that sulfated oligosaccharides, such as glycosaminoglycans (GAGs), near the membrane surface may act as a potential target to enhance the penetration of amphiphilic CTXs through membrane lipid bilayers (*4*). This hypothesis is supported by the observation that heparin may enhance the aggregation of CTX molecules and also promote its penetration into monolayer membranes. In addition, GAGs bind to homologous CTXs with different specificity (*5*). For instance, the binding strength of CTX Tγ, a major component of the venom from spitting cobra *Naja nigricollis*, to various GAGs is significantly different from that of CTX A3, a major component of the venom from Taiwan cobra *Naja atra*. This effect provides a simple explanation to account for the action of CTX Tγ from spitting cobra causing corneal opacity and/or blindness, in addition to the systolic heart arrest caused by CTXs in general (*5*). Although it remains to be established whether CTX action at the cellular level is indeed affected by GAGs in the extracellular matrix, CTX−GAG interactions may serve as an interesting model system for understanding the binding specificity of proteins against GAGs.

Analysis of binding of CTXs to heparin by circular dichroism, fluorescence spectroscopy, and molecular modeling has suggested that the CTX−GAG complex is formed by the cationic belt of the conserved residues on the concave surface of three-finger β-sheet polypeptides initiating ionic interaction with GAG molecules followed by specific binding

† This work was supported by NHRI Grant EX90-8810BL and NSC Grant 89-2311-B-007-045 and an NSC-NRC Joint Research Project Grant (N-001).

* To whom correspondence should be addressed. E-mail: wgwu@life.nthu.edu.tw. Fax: +886 3 5715934. Tel: +886 3 5742752.

§ Department of Life Sciences, National Tsing Hua University, Hsinchu 30043, Taiwan.

‡ Institute for Biological Sciences, National Research Council, Ottawa, K1A OR6, Canada.

[1] Abbreviations: CTX, cardiotoxin; GAG, glycosaminoglycan; NMR, nuclear magnetic resonance; IdoA2S, 2-*O*-sulfo-α-L-idopyranosyluronic acid; IdoA, iduronic acid; ΔUA, uronic acid; GlcNS6S, 2-amino-2-deoxy-2,6-disulfo-α-D-glucopyranose; GlcN, glucosamine; FGF, fibroblast growth factor; FPLC, fast performance liquid chromatography; TOCSY, total correlation spectroscopy; NOESY, nuclear Overhauser effect spectroscopy; trNOE, transferred nuclear Overhauser effect; 1D ge-TOCSY, one-dimensional gradient-enhanced total correlation spectroscopy; 1D ge-NOESY, one-dimensional gradient-enhanced nuclear Overhauser effect spectroscopy; CORCEMA, complete relaxation and conformational exchange matrix analysis; q-SNEEZE, quiet suppression via extremely even z excitation.

10.1021/bi010847n CCC: $20.00
Published on Web 08/10/2001

of lysine residues near loop II of CTX (*6*). Several observations were derived from these studies. First, about two-thirds of the positively charged residues are located at the concave side. Second, a single amino acid mutation near the N-terminus located at the concave side changes the apparent dissociation constant, K_d, of the CTX−heparin complex. Third, comparison of the GAG binding strength and specificity of 10 CTX homologues indicated that those Lys/Arg residues located on the concave side are involved. However, Lys5 located at the convex side of CTX appears to play a role in affecting the aggregation state of the CTX−heparin complex since higher concentrations of heparin can reverse the heparin-induced aggregation of the CTX−heparin complex for CTXs consisting of Arg/Lys5 (*6*). The molecular details of CTX−GAG interactions that account for the binding specificity and heparin-induced aggregation, however, have not been studied by spectroscopic techniques and remain to be elucidated.

Heparin-induced oligomerization of proteins is a general phenomenon for many GAG binding proteins (*7*−*13*). It received much attention as a result of recent structural analyses on complexes of fibroblast growth factors (FGFs) with heparin fragments or heparin analogues (*14*−*16*). It is well established that binding of heparin to FGF induces FGF assembly along the GAG chain and the oligomerized FGF plays a functional role at the cellular level (*12*, *17*, *18*). The regulation of heparin-induced oligomerization of proteins is, therefore, an important issue in understanding the structure−function relationship of GAG binding proteins. Since the aggregation and dissociation of CTXs appear to be regulated by the binding of heparin alone, as shown for the case of heparin-induced aggregation of both CTX Tγ and CTX A3, the understanding of this interaction in detail may shed light on other GAG binding proteins which exhibit similar aggregation properties. Therefore, in this study, a detailed NMR structural analysis of the heparin binding site of both CTX A3 and Tγ and of the bound conformation of heparin-derived polysaccharide under nonaggregated conditions was performed to elucidate the nature of the saccharide−toxin interaction.

EXPERIMENTAL PROCEDURES

Preparation of Heparin-Derived Polysaccharides. Porcine intestinal heparin (100 mg) was depolymerized with 40 mIU *Flavobacterium* heparinase I (Sigma, catalog no. H-2519) in a 1 mL reaction buffer as described previously (*19*). Successive enzymatic depolymerization gave various heparin-derived polysaccharides with different chain lengths (from disaccharide to octadecasaccharide). These fragments were further purified with a P-10 gel filtration column according to their respective molecular sizes. A Sephadex G-15 gel filtration column was used for final desalting. Average molecular weights and corresponding carbohydrate chain lengths were estimated using gradient polyacrylamide gel electrophoresis and mass spectrometry (*20*). The analysis of the sample purity by electrophoresis and FPLC indicated that the heparin-derived disaccharide sample included one major compound (>90%). Further purification by FPLC yielded the pure fully sulfated heparin-derived disaccharide used in this study (Figure 1). The structure of fully sulfated disaccharide was confirmed by comparing its spectrum with the known proton NMR spectrum of the commercial standard

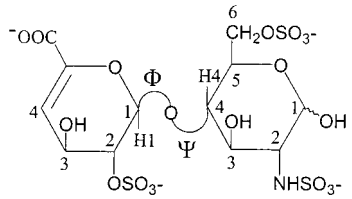

b: ΔUA2S a: GlcNS6S

FIGURE 1: Chemical structure of the fully sulfated heparin-derived disaccharide. Residues are labeled a for glucosamine and b for uronic acid. The torsion angles for the glycosidic linkage are defined by Φ ($H1^b-C1^b-O-C4^a$) and Ψ ($C1^b-O-C4^a-H4^a$).

compound (Sigma, catalog no. H-9267). The other three kinds of monosulfated heparin disaccharides used in this study were purchased from Sigma (catalog nos. H-9017, H-9142, and H-1145). However, heparin-derived tetra- and hexasaccharides obtained according to the aforementioned procedure, containing 6−12 components with different sulfation patterns were used in experiments directly without any further purification.

Purification of Cardiotoxin and Preparation of NMR Samples. Cardiotoxin A3 and Tγ were purified from the cobra venom of *N. atra* and *N. nigricollis* (purchased from Sigma), respectively, by SP-Sephadex C-25 ion exchange column chromatography and further by using a reverse-phase C-18 (10 mm) HPLC column as described previously (*21*). The oligosaccharides and toxins were dissolved in 500 μL of a 90% H_2O/10% D_2O mixture or 100% D_2O containing 10 mM phosphate buffer at the desired sugar/protein ratios (see the text), and the sample pH was adjusted to 6.0 by titrating with NaOH or HCl after considering the isotope effect with pD = pH* + 0.4 (for 100% D_2O only). The sample for determining the bound conformation of the heparin disaccharide was set to a protein/sugar ratio of 1/1 (5 mM/5 mM), which was confirmed by integration of the NMR resonances of the sugar and the protein.

Protein Chemical Shift Variation Analysis. The comparisons of protein chemical shifts were performed by two-dimensional (2D) NMR experiments carried out on a Bruker DRX600 and DMX500 spectrometer at 27 °C. The 2D TOCSY spectra with a mixing time of 90 ms and the NOESY spectra with a mixing time of 150 ms were recorded by using time-proportional phase increments (*22*, *23*). Water suppression was achieved by pulsed field gradients with the 3−9−19 WATERGATE sequence. The chemical shift was referenced to 4,4-dimethyl-4-silapentane sodium carboxylate (DSS) at 0.015 ppm. All spectra were typically acquired with 2048 complex data points in the t_2 dimension and 512 points in the t_1 dimension. Data processing was carried out on a Silicon Graphics O2 workstation using the XWINNMR program.

One-Dimensional Selective Homonuclear Experiments. The conformation of the heparin disaccharide was investigated using one-dimensional (1D) selective experiments, (1D ge-TOCSY, 1D ge-NOESY, and 1D ge-TOCSY-NOESY) on a Varian INOVA600 spectrometer (*24*). 1D ge-TOCSY was used to assign the proton resonances of the disaccharide, and 1D ge-NOESY was used to acquire the NOE information. When necessary, 1D ge-TOCSY-NOESY with double selection was used to extract the NOE data of the protons buried within the protein signals, for instance, $H4^a$ and $H2^b$.

1D ge-TOCSY-NOESY is the 1D analogue of the three-dimensional (3D) homonuclear technique, derived by combining the building blocks of 1D ge-TOCSY and 1D ge-NOESY (*25*). The implementation of a z-filter can suppress the ROE effect during the TOCSY spin-lock sequence (*26*). The on-resonance q-SNEEZE pulse (appropriate bandwidth from 20 to 200 Hz) was chosen as a selective 90° pulse and applied on the peak to be observed (*27*). The power level and pulse length were generated according to the product of bandwidth (BW in hertz) and pulse length (PW in seconds) such that BW × PW = 4.85. Purging pulsed field gradients (PFGs) were used rather than coherence selection in all experiments. The proton carrier frequency was set at the HOD resonance, and experiments were performed at 25 °C. 1D ge-NOESY and 1D ge-TOCSY-NOESY spectra were acquired to obtain NOE buildup curves with 10 NOE mixing times ranging from 100 to1000 ms with 100 ms increments and 1024 scans each. The NOE intensities were normalized against the excited peaks decay which was fitted to an exponentially decaying function and extrapolated back to an intensity of 100% at zero mixing time. The *J* coupling constants were also measured via 1D ge-NOESY and 1D ge-TOCSY by using the spectral deconvolution function of standard Varian VNMR software.

Conformational Analysis. The program CORCEMA, which was designed to calculate theoretical NOE or ROE values for the case with multistate conformational exchange, was used to determine the conformations of heparin disaccharide with or without CTXs (*28*, *29*). The two-mode system, as mentioned by Moseley (*28*), was used here assuming the sugar will undergo only a two-state conformational change described by the bound and free conformations. The exchange was simply described by the dissociation constant between sugar and protein (K_d) and the on and off (k_{on} and k_{off}, respectively) with the relationship $K_d = k_{off}/k_{on}$. The distances of the intraresidue proton pairs of glucosamine are already known as good distance standards when determining the heparin structure because the ring conformation of glucosamine always maintains its $^4C_1$ conformation. The H1^a/H2^a proton pair of glucosamine with a fixed distance (2.45 Å) was chosen as a reference for comparison with the calculated data from CORCEMA. Iterative fitting was adopted to optimize all parameters, including k_{on}, k_{off}, correlation times of the bound and free forms, concentrations, and the leakage factor, to obtain the best fit between CORCEMA data and experimental results. The quality of the fit was judged by the value of the *R*-factor (*30*, *31*), defined by the equation

$$R = \sqrt{\frac{\sum_i (I_{i,\mathrm{exp}}/I_{\mathrm{ref,exp}} - I_{i,\mathrm{cal}}/I_{\mathrm{ref,cal}})^2}{\sum_i (I_{i,\mathrm{exp}}/I_{\mathrm{ref,exp}})^2}}$$

where I_i is the NOE cross-peak intensity at various mixing time and I_{ref} is the intensity of the H1^a/H2^a reference peak. The glycosidic torsion angles were changed in 1° steps to determine the conformation with the minimum averaged *R*-factors. All calculations were performed on a SGI O2 workstation.

Molecular Modeling of the Complex. Molecular modeling was conducted using Discovery 3.0 of Insight II 95.0 on a SGI O2 workstation. The AMBER force field with Homans addition (*32*) and sulfate parameter extension (*33*) for saccharides was chosen to define the charge distribution and interaction energies in all calculations. The bound disaccharide structure derived from CORCEMA analysis was docked on the predicted binding site of A3 manually. The whole complex was then soaked with a 5 Å water layer. The nonbonded cutoff value was set at 15 Å, and an energy minimization with 300 steps was performed initially to remove improper atom contacts and forces. A 50 ps molecular dynamics simulation was performed with a time step of 1 fs, and the coordinates of the complex were saved in a trajectory file for the final analysis.

RESULTS

Heparin Binding Site of CTX A3 under Nonaggregated Conditions. To identify the heparin binding site and determine the structure of the heparin−CTX complex by using high-resolution NMR, one needs to avoid the heparin-induced aggregation of the samples. CTX A3 has been shown previously to aggregate in the presence of both high-molecular weight ($M_r \sim 15000$) and low-molecular weight ($M_r \sim 3000$) heparins (*6*), indicating that a heparin chain length as high as a decasaccharide (assuming an average molecular weight of ∼350 for disaccharide repeats without sulfation or of ∼570 with three sulfations) can cause significant aggregation. The sulfated pentasaccharide has been proposed to be sufficient for binding to CTX. To probe more completely the requirements for heparin oligosaccharide binding to CTX, the binding of di-, tetra-, and hexasaccharides obtained from enzymatic depolymerization was further investigated. Most of the heparin molecule is formed by a repeating disaccharide unit consisting primarily of 2-amino-2-deoxy-2,6-disulfo-α-D-glucopyranose (α-D-GlcNS6S) and 2-*O*-sulfo-α-L-idopyranosyluronic acid (α-L-IdoA2S). It should be emphasized that heparinase depolymerization produces, at the reducing end, a terminal uronate with an unsaturated 4,5 carbon bond (ΔUA). Thus, the pure fully sulfated disaccharide compound used in this study is ΔUA2S(1→4)-α-D-GlcNS6S (Figure 1).

All three heparin-derived di-, tetra-, and hexasaccharides can be seen to bind in a fashion similar to that of CTX A3 as judged by the ^{1}H chemical shift perturbation of both amide proton and C_α proton resonances of CTX A3 (Figure 2). The sugar/protein ratios of all NMR samples were carefully controlled to prevent aggregation. The chemical shift variations of all 60 amino acid resonance positions for the three samples are similar with the most significant perturbation centered at the same Cys38 position. Other significant perturbations can also be detected for the NH and C_αH resonances of Leu6 and Tyr22, and Lys5 and Lys23, respectively.

An NMR titration experiment with CTX A3 against increasing concentrations of the heparin disaccharide was then performed by monitoring the NMR resonances exhibiting the most significant perturbation. As shown in Figure 3A, the heparin disaccharide induced chemical shift variations in a dose-dependent manner. All the titration curves in Figure 3A could be fitted by a single dissociation constant of 1.05 mM, suggesting that all the studied amide chemical

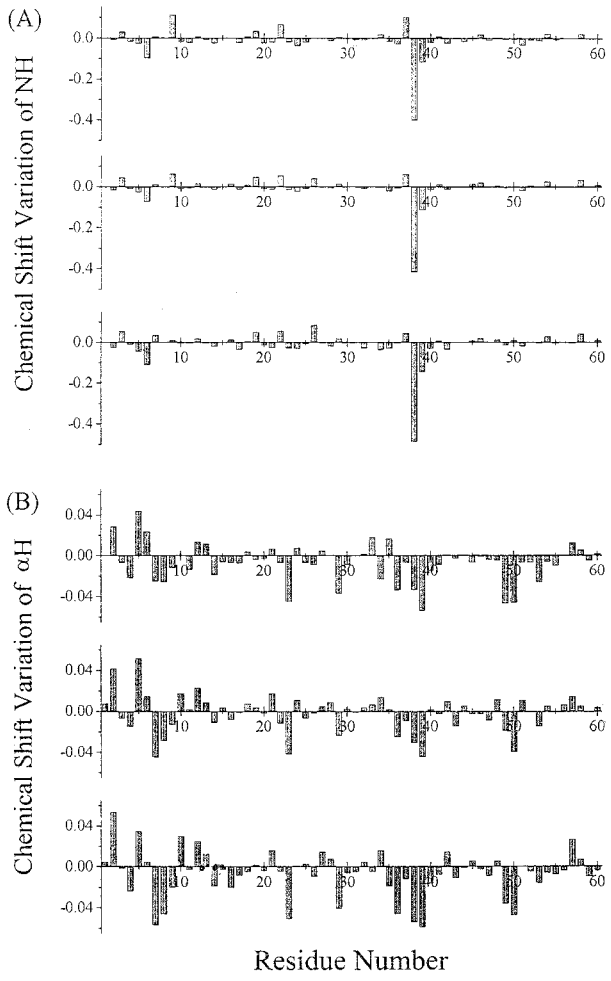

FIGURE 2: Summary of proton chemical shift differences for CTX A3 (5 mM in 10 mM phosphate buffer at pH 6.0) in the presence and absence of a heparin-derived fragment at 27 °C. (A) Variation measured for the NH resonances and (B) variation measured on $C_\alpha H$ resonances from the sample of 1/2 A3/disaccharide ratio, 2/1 A3/tetrasacchride ratio, and 2/1 A3/hexasaccharide ratio (from top to bottom).

shift variation might be associated with the same heparin binding site of the CTX A3 molecule. It also shows that the binding stoichiometry of the disaccharide−CTX complex is ~1/1.

The disaccharide−CTX complex was found to be the most suitable for NMR experiments. Significant aggregation of CTX A3 induced by heparin-derived tetra- and hexasaccharide could readily be observed as judged by the line broadening effect in 2D spectra and the increased turbidity of the samples in the NMR tubes after increasing the concentration of heparin fragments. In fact, even at CTX concentrations as low as 10 μM, both tetra- and hexasaccharide samples can be seen to induce visible aggregation as judged by the increase in the relative scattering intensity of the sample (Figure 3B). The phenomena indicated the difficulty of performing NMR experiments at higher ratios of the heparin-derived tetra- and hexasaccharide−CTX A3 complexes. However, the NMR sample for the complex of the heparin-derived disaccharide and CTX A3 stayed transparent throughout the entire experimental time span (up to 1 week) and showed no indication of aggregation as monitored by light scattering measurement, in contrast to the behavior of the tetra- and hexasaccharide complexes.

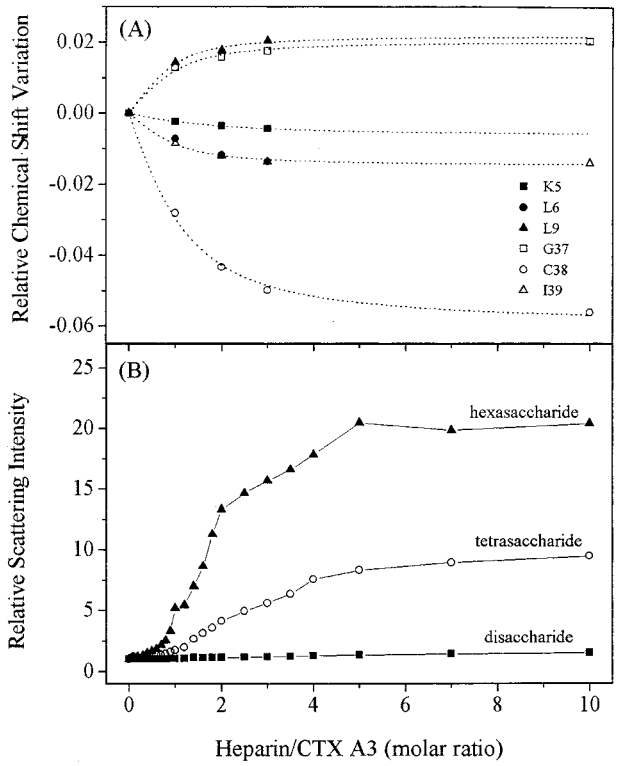

FIGURE 3: (A) Titration curve of CTX A3 (2 mM) against the heparin-derived disaccharide. The relative chemical shift variations of six amide protons of protein residues, K5 (■), L6 (●), L9 (▲), G37 (□), C38 (○), and I39 (△), were chosen for measuring the binding constant. The dotted lines represent the least-squares fit of experimental data using a binding constant of 1.05 mM. (B) Change of relative scattering intensity of CTX A3 (10 μM) against different molar ratios of disaccharide, tetrasaccharide, and hexasaccharide. The excitation wavelength was set at 280 nm, and the scattering intensity was observed at the same wavelength.

In view of the similarity of the chemical shift variations for the di-, tetra-, and hexasaccharide samples, it was concluded that all the ^{1}H NMR data shown in Figures 2 and 3 mainly reflect only one heparin−CTX A3 binding site under nonaggregated conditions. Hence, since the disaccharide was found to be the most suitable sample for NMR measurements, the following experiments focused on the binding behavior between the heparin-derived disaccharide and CTXs.

Similar Heparin Binding Site of CTX A3 and Tγ. In light of a single heparin binding site for CTX A3 under nonaggregated conditions, it is interesting to see whether a similar conclusion can also be drawn for other CTX proteins exhibiting different binding specificities and behavior. CTX Tγ from *N. nigricollis* has been shown to exhibit weaker binding than CTX A3 to long chain heparin, based on circular dichroism and fluorescence spectroscopic binding measurements (*6*). As shown in Figure 4, the patterns of chemical shift variation of the NH and $C_\alpha H$ resonances for both CTX A3 and Tγ are similar, indicative of a similar heparin binding site for the two proteins. The main differences in chemical shift variation between the two proteins occurred for positions Leu6, Tyr22, and Cys38. Differences in binding could be due to the positively charged amino acid substitutions at positions 5, 16, 27, and 31 (Figure 4).

NMR Structures of Heparin-Derived Disaccharide in the Presence and Absence of CTXs. The conformation of the

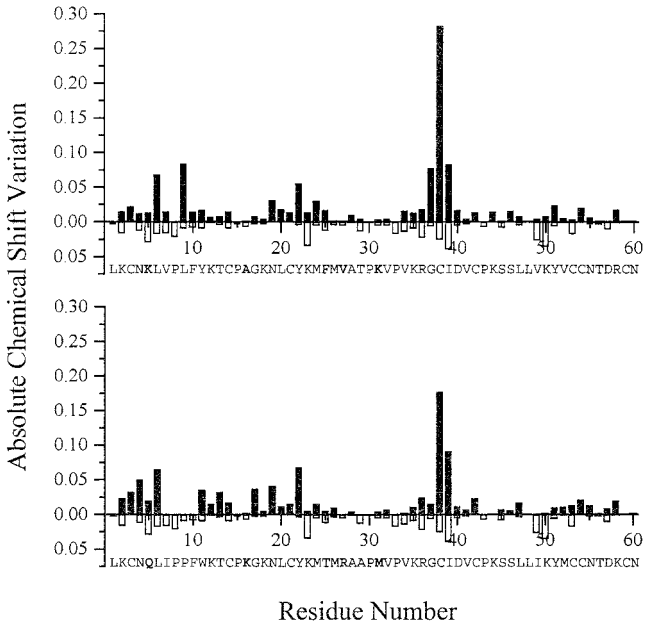

FIGURE 4: Absolute chemical shift variation of NH (black columns) and $C_\alpha H$ (white columns) resonances of A3 (top) and CTX Tγ (bottom) in the presence and absence of disaccharide. An equimolar CTX/sugar ratio (2 mM/2 mM) was used. The sequences of two CTXs are below the amino acid numbers. Changes in the positively charged amino acid residue (Gln5 vs Lys5, Lys16 vs Ala16, Arg27 vs Val27, and Met31 vs Lys31) are listed in bold.

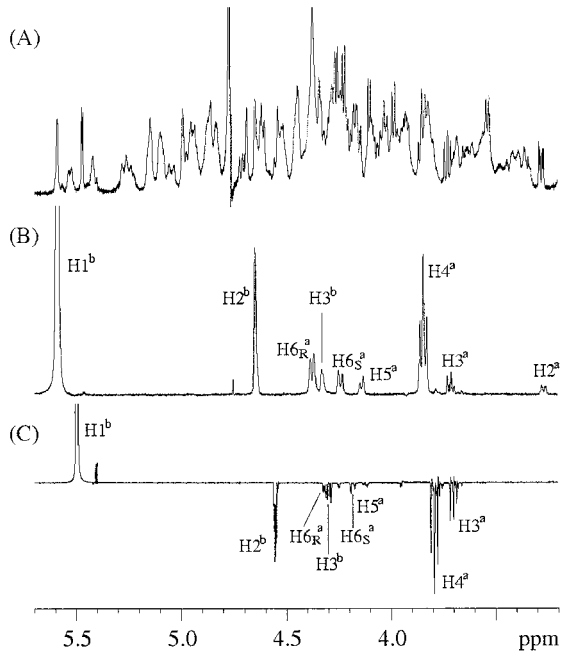

FIGURE 5: 1D proton spectrum (A), 1D selective NOESY spectrum of a 1/1 CTX A3−disaccharide complex (B), and 1D selective NOESY spectrum of free disaccharide (C) performed at 25 °C. The 20 Hz on-resonance excitation band generated by a q-SNEEZE pulse was centered at the $H1^b$ resonance. The NOE peaks are negative for the free form and positive for the complex indicating binding.

heparin disaccharide bound to CTX A3 in solution was determined using a 1/1 protein/sugar ratio. Due to the low molecular weight of CTX A3 (~7000), it was possible to work at a 1/1 ratio where both protein and sugar resonances can be clearly observed, along with transferred and intermolecular NOEs.

By using a combination of full relaxation and conformational exchange matrix analysis of ^{1}H NOE data, the solution conformation of a homogeneous heparin-derived tetrasaccharide in the presence and absence of the plasma protein antithrombin has been recently reported (*34*). In this study, a similar approach was adopted using selective 1D ge-NOESY spectra (Figure 5) for the generation of the NOE buildup curves (Figure 6). As shown in Figure 5, selective excitation allowed the determination of NOEs with improved sensitivity and resolution. For the free heparin disaccharide, the signs of the NOE peaks are negative, due to the fast tumbling rate of the molecule. Upon binding to CTX A3, the NOE peaks are positive, an indication that the molecule is indeed bound to and tumbling with CTX A3 at a slower tumbling rate.

Significant chemical shift changes can also be detected for the heparin-derived disaccharide in the presence and absence of CTX A3 or Tγ (Table 1). For instance, as shown in the binding study of the heparin disaccharide with CTX A3 (compare panels B and C of Figure 5), the most significant effects can be seen for $H1^b$ and $H2^b$ of ΔUA2S, although $H3^b$ located in the same carbohydrate moiety exhibits only a small perturbation. This indicated that either the ring conformation of ΔUA2S and/or the glycosidic bond between ΔUA2S and GlcNS6S had undergone significant change. Interestingly, binding of CTX Tγ to the heparin disaccharide produces only about half of the chemical shift change for $H1^b$ and $H2^b$ as compared to binding of CTX A3. It suggests that CTX Tγ perturbed to a smaller extent of the conformation of the heparin-derived disaccharide upon binding. As discussed below, structure determination of the heparin-derived disaccharide based on NOE information gave further support for this conclusion.

Proton *J* coupling constants are known to be useful in deriving the average conformation of the carbohydrate ring and providing insights into the conformational equilibrium. As shown in Table 2, *J* values determined by ^{1}H selective 1D ge-TOCSY and 1D ge-NOESY spectra also exhibited significant change for the heparin-derived disaccharide under different binding conditions. Again, the perturbation is generally larger for the CTX A3−heparin-derived disaccharide complex than for the CTX Tγ−heparin-derived disaccharide complex. A monotonic decrease in the $J_{1,2}$ and $J_{2,3}$ coupling values in ΔUA2S and of $J_{5,6R}$ and $J_{5,6S}$ in GlcNS6S can clearly be seen for the free form, bound form with CTX Tγ, and bound form with CTX A3 of the heparin-derived disaccharide.

$J_{1,2}$ and $J_{2,3}$ in the unsaturated uronic acid have been proposed to represent the relative population of two energy-favored conformers, $^1H_2$ and $^2H_1$ (*35*). In the same report, $J_{1,2}$ and $J_{2,3}$ values of 2.87 and 2.37 Hz for the $^1H_2$ conformer and 8.27 and 7.67 Hz for the $^2H_1$ conformer, respectively, were proposed. The changes in $J_{1,2}$ and $J_{2,3}$ after binding to the two kinds of CTXs were a strong indicator that the sugar ring of ΔUA2S converted fully to the $^1H_2$ conformation. $J_{5,6R}$ and $J_{5,6S}$ in GlcNS6S are also interesting since they indicated that either the dynamic or the conformation of the 6-*O*-sulfated side chain was perturbed. The 6-*O*-sulfate orientation is determined by the three eclipsed C5−C6 conformers, *gg*, *gt*, and *tg* [gauche (*g*) or trans (*t*)], defined by the two dihedral angles, $H5-C5-C6-H6_S$ and $H5-C5-C6-H6_R$ (*36*). In the absence of CTXs, the 6-*O*-sulfate group exists

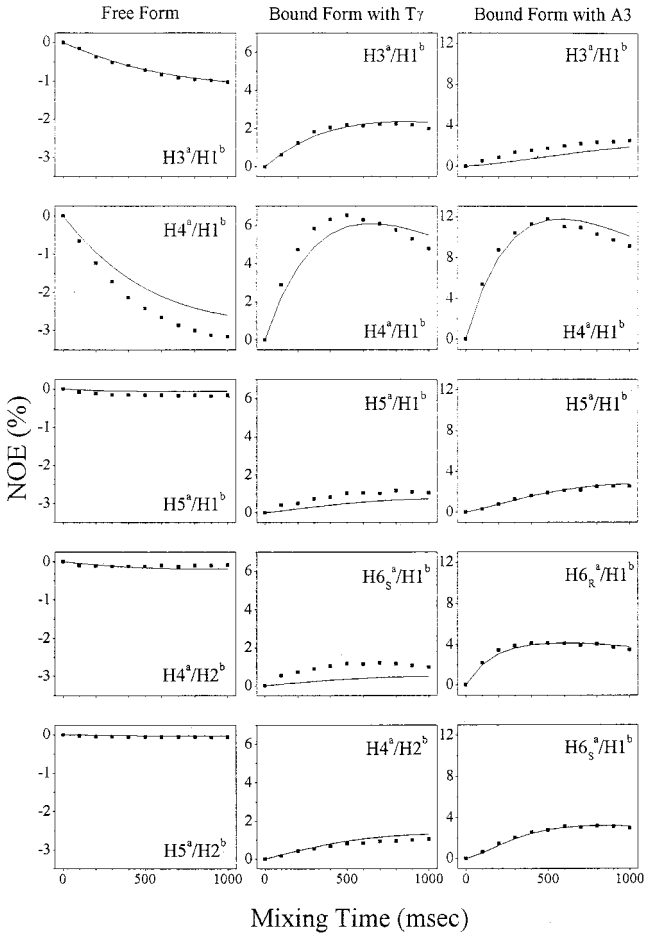

FIGURE 6: Comparison of the experimental interglycosidic transferred NOEs for the free disaccharide (left column), bound disaccharide with CTX Tγ (middle column), and bound disaccharide with A3 (right column). The solid lines were calculated using CORCEMA with the parameters given in Table 3.

Table 1: ^{1}H Chemical Shifts[a] of the Heparin-Derived Disaccharide in Aqueous Solution, δ_{free}, and in the Presence of CTX Tγ (1/1), $\delta^{T\gamma}{}_{bound}$, and A3 (1/1), $\delta^{A3}{}_{bound}$

	δ_{free}	$\delta^{T\gamma}{}_{bound}$	$\delta^{A3}{}_{bound}$	$\delta^{T\gamma}{}_{bound-free}$	$\delta^{A3}{}_{bound-free}$
H1ᵃ	5.454	5.484	5.487	0.030	0.033
H2ᵃ	3.280	3.298	3.295	0.018	0.015
H3ᵃ	3.763	3.787	3.741	0.024	0.022
H4ᵃ	3.829	3.857	3.871	0.028	0.042
H5ᵃ	4.160	4.175	4.176	0.015	0.016
H6Sᵃ	4.214	4.239	4.271	0.025	0.057
H6Rᵃ	4.350	4.377	4.404	0.027	0.054
H1ᵇ	5.503	5.563	5.620	0.060	0.117
H2ᵇ	4.574	4.616	4.677	0.042	0.103
H3ᵇ	4.343	4.377	4.356	0.034	0.013
H4ᵇ	5.974	6.028	6.048	0.054	0.074

[a] Measured by 1D ge-TOCSY and 1D ge-NOESY at 25 °C and 100% D_2O, with an estimated error of ±0.002 ppm.

in a *gt* and *gg* equilibrium. After binding to CTXA3 takes place, $J_{5,6R}$ and $J_{5,6S}$ had smaller values of 2.64 and 1.84 Hz, respectively, showing that the 6-*O*-sulfated side chain had undergone a change in orientation, corresponding to a 100% *gg* conformer. In contrast, binding to CTX Tγ induces no significant changes in either $J_{5,6R}$ or $J_{5,6S}$ values. In addition, the ^{1}H chemical shifts of H6Sᵃ and H6Rᵃ in GlcNS6S were perturbed the most upon disaccharide binding to CTX A3 (Table 1).

Table 2: Vicinal Proton Coupling Constants[a] of the Heparin-Derived Disaccharide in Aqueous Solution and in the Presence of CTX Tγ (1/1) and A3 (1/1)

	GlcNS6S						ΔUA2S		
	$J_{1,2}$	$J_{2,3}$	$J_{3,4}$	$J_{4,5}$	$J_{5,6R}$	$J_{5,6S}$	$J_{1,2}$	$J_{2,3}$	$J_{3,4}$
disaccharide only	3.4	10.3	9.2	9.5	4.0	2.2	3.4	2.7	4.4
Tγ complex	3.4	10.2	9.1	9.6	4.0	2.3	2.8	2.3	4.6
A3 complex	3.4	10.4	9.1	10.2	2.6	1.8	2.5	2.0	4.7

[a] Measured by 1D ge-TOCSY at 25 °C and 100% D_2O, with an estimated error of ±0.1 Hz.

Table 3: Optimized Parameters Used in CORCEMA Calculations and Corresponding *R*-Factors

	free form (Φ = 26°, Ψ = −77°)	bound form with Tγ (Φ = 28°, Ψ = −76°)	bound form with A3 (Φ = 64°, Ψ = −5°)
input parameters			
correlation time (ns)	0.12	4.0	3.8
K_d (mM)	−	3.2	1.0
k_{on} (s^{-1} M^{-1})	−	1×10^7	1×10^5
k_{off} (s^{-1})	-	3.2×10^4	1×10^2
6-SO_4 orientation	gt	gt	gg
ring conformation	85% $^1H_2$, 15% $^2H_1$	100% $^1H_2$	100% $^1H_2$
R-factors of trNOE			
H1ᵃ/H2ᵃ	0.109	0.075	0.096
H3ᵃ/H1ᵇ	0.040	0.085	0.390
H4ᵃ/H1ᵇ	0.203	0.113	0.068
H5ᵃ/H1ᵇ	0.636	0.443	0.069
H6Rᵃ/H1ᵇ	−	−	0.054
H6Sᵃ/H1ᵇ	−	0.654	0.044
H4ᵃ/H2ᵇ	0.555	0.243	−
H5ᵃ/H2ᵇ	0.593	−	−
average[a]	0.405	0.308	0.125

[a] Values averaged only from the interglycosidic proton pairs.

To determine the exact conformational change of the heparin-derived disaccharide in the presence and absence of CTX molecules, complete relaxation and conformational exchange matrix (CORCEMA) analysis of the NOE buildup curves was performed (Figure 6). The optimized parameters using CORCEMA calculations and the corresponding *R*-factors, which indicate the deviation between the theoretical and experimental values, are shown in Table 3. The optimized glycosidic angles, Φ and Ψ, for the bound and free forms as defined in Figure 1 are also given. It is noteworthy that the correlation times, 3.8−4.0 ns, derived by the CORCEMA analysis for the CTX-bound disaccharide are in close agreement with the overall correlation time of 4.5 ns determined for CTX A3 from ^{13}C relaxation studies (*37*). Such agreement is taken as validation of the results of the NOE analysis and, thus, supporting conclusions drawn from the analysis.

Four results derived from this study of the bound sugar conformation for the heparin−CTX complex are noteworthy. First, although the glycosidic angles (Φ and Ψ) for the free heparin-derived disaccharide form (26° and −77°, respectively) are significantly perturbed when bound to CTX A3 (64° and −5°, respectively), it remains similar when bound to CTX Tγ (28° and −76°, respectively). Second, the K_d value of the CTX Tγ−heparin-derived disaccharide complex (3.2 mM) is only slightly higher than that of the CTX A3−heparin-derived disaccharide complex (1 mM), but both the on-rate and off-rate of heparin-derived disaccharide are

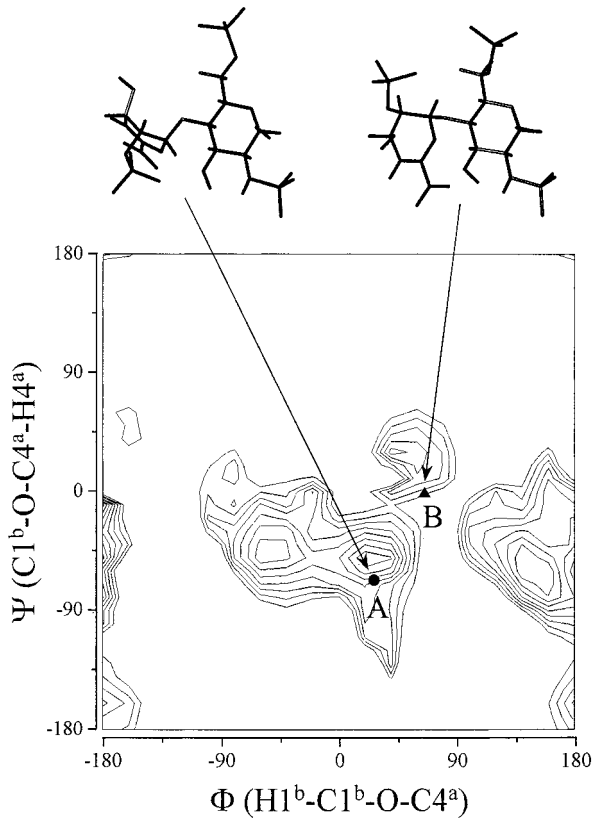

FIGURE 7: Φ−Ψ energy map of the disaccharide using the modified AMBER force field. Ten iso-energy contours are draw by interpolation of 1.5 kcal/mol above the global minimum. The Φ and Ψ angles of two bound forms binding with CTX Tγ and A3 calculated from CORCEMA are indicated in the map by the A and B labels, and the corresponding conformations are drawn on top.

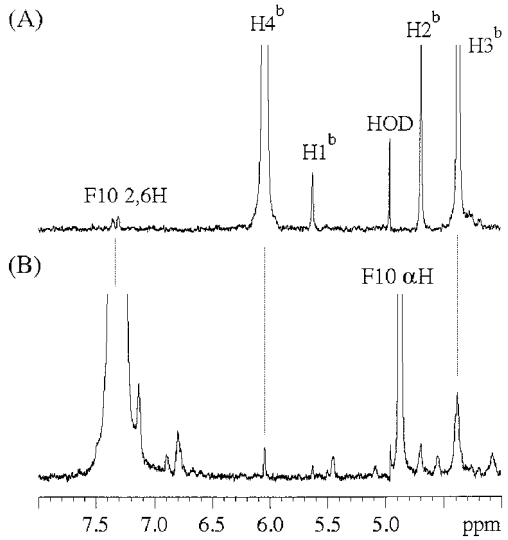

FIGURE 8: Intermolecular NOE between A3 and the disaccharide identified by 1D selective NOESY for H4^b (A) and for 2,6H of F10 (B) with a CTX A3/disaccharide ratio of 1/1 (5 mM/5 mM) at 10 °C. The dotted lines indicate intermolecular NOEs. The assignments of the proton resonances with significant NOEs are also labeled.

almost 2 orders of magnitude higher for CTX Tγ than for CTX A3. Third, the 6-*O*-sulfated side chain of the bound form of GlcNS6S with CTX A3 adopted the *gg* conformer, in contrast to the *gt*−*gg* equilibrium present in the free form and the bound form with CTX Tγ. Fourth, the ring conformation of ΔUA2S changed to the $^1H_2$ form upon binding to CTX A3 and CTX Tγ, but it is in equilibrium between the $^1H_2$ and $^2H_1$ forms for free disaccharide.

The two NOE-determined conformations (A and B) of the heparin disaccharide were further compared with the Φ−Ψ energy contour map generated by using the modified AMBER force field (Figure 7). Conformation A of the free heparin-derived disaccharide is situated reasonably close to one of the four energy minima located with Φ and Ψ values of 26° and 60°, respectively. The CTX A3-induced conformation B apparently is closer to the other energy minimum with Φ and Ψ values of 45° and 30°, respectively. The conformation of the glycosidic linkage based purely on the geometric constraint using CORCEMA analysis can therefore be considered to be reasonable.

It should be emphasized that the solution conformation of the free disaccharide is not represented by one conformation only, but it is sampling multiple conformations. For simplicity, the NOE analysis of the free form was carried out using only one conformation which gives NOEs similar to those of the ensemble population. The bound conformation with CTX A3 is expected to be due to one conformation since the ΔUA2S ring has also changed conformation and the NOEs are very different between the bound and free forms. For the bound conformation with CTX Tγ, the linkage conformation and the ΔUA2S ring could still be averaging between multiple conformations, since there were no changes in the glycosidic torsion angles for the bound form and free form, and the coupling constants for this ring indicated flexibility. Hence, the bound form could still be an ensemble average of multiple conformations found in solution with only the GlcNS6S ring bound. Due to more conformational averaging for the free form and the bound form with CTX Tγ, their *R*-factors in Table 3 are larger than the one for the bound form with CTX A3, since flexibility is not taken into account in the CORCEMA calculations.

Structure of the CTX A3−*Heparin-Derived Disaccharide Complex.* Intermolecular NOEs between the sugar and protein could be observed. Due to the low molecular weight of CTX A3, it was possible to work at a 1/1 ratio where both protein and sugar resonances could be clearly observed. Hence, in conjunction with the chemical shift analysis upon binding, the structure of the complex under nonaggregated conditions could be determined using molecular docking methods. As pointed out before, CTX is a slightly curved β-sheet molecule with N- and C-termini located at the concave side. Most of the lysine residues are located on the concave side and form a positively charged cradle suitable for long chain heparin binding. However, under our current nonaggregated experimental condition, the most significantly perturbed residue, Cys38, is located at the convex side. Although it is possible to identify the heparin binding site as being near the interface between loop I and loop II based on the chemical shift perturbation, it remains to be decided whether the binding occurs on the *concave* or the *convex* side.

As shown in Figure 8, an unambiguous intermolecular NOE of 0.3 ± 0.1% was observed between the 2,6 proton resonances of Phe10 and the H4^b resonance of ΔUA2S. The selective excitation of the H4^b resonance of ΔUA2S gives rise to a detectable NOE for the 2,6H of Phe10 signal (Figure 8A), and the excitation of the 2,6H resonances of Phe10 also

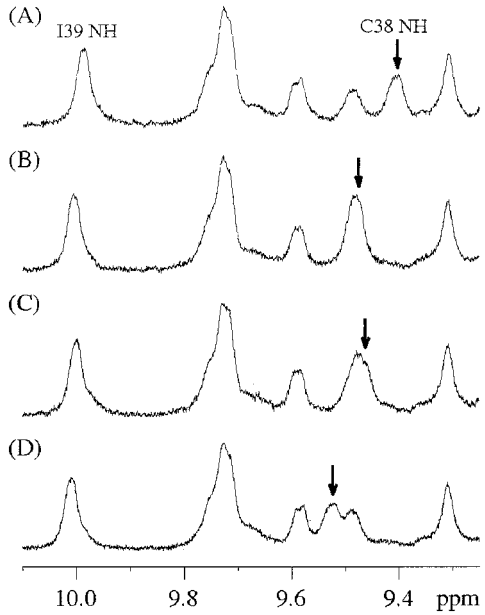

FIGURE 9: Proton NMR spectra indicating the changes in chemical shift for the NH resonance of C38 (indicated by arrows) and I39 of CTX A3 after equimolar addition (1 mM) of different heparin-derived monosulfated disaccharides, ΔUA-GlcNS (A), ΔUA2S-GlcN (B), and ΔUA-GlcN6S (C). The proton spectrum of CTX A3 is shown in panel D. All experiments were performed in 10 mM phosphate buffer, 90% H_2O, and 10% D_2O at pH 6 and 10 °C.

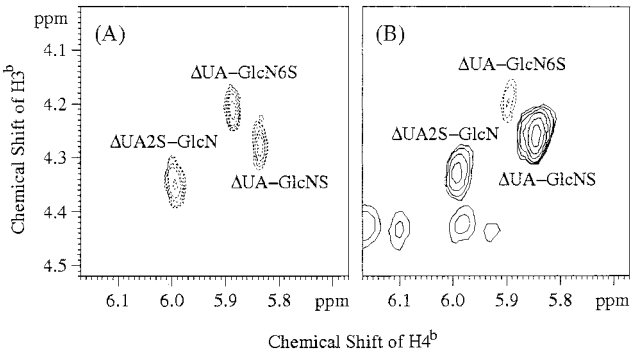

FIGURE 10: 2D NOESY spectra of the GlcN $H3^b/H4^b$ cross-peaks for an equimolar (1 mM) mixture of three disaccharides, ΔUA-GlcNS, ΔUA2S-GlcN, and ΔUA-GlcN6S, in the absence (A) and presence of equimolar CTX A3 (B). With respect to the positive diagonal peaks, the NOE peaks in panel B for the disaccharide bound to CTX A3 are positive (—) while a negative NOE peak (•••) indicates weak binding. The NOE peaks for the disaccharide mixture with no CTX are negative (A). Extra positive protein cross-peaks in panel B are also observed. All experiments were performed in 10 mM phosphate buffer and 100% D_2O at pH 6 and 10 °C with an NOE mixing time of 600 ms.

produces intermolecular NOEs for $H3^b$ and $H4^b$ of ΔUA2S (Figure 8B). Since the side chain of Phe10 is located at the convex side of the CTX A3 molecule, it suggests that the heparin-derived disaccharide indeed binds at the convex side with the ΔUA2S ring closer to loop I of the molecule.

The large chemical shift variation of the NH resonance of C38 due to heparin binding also provided a tool for determining the exact sulfate residue involved in the binding. By addition of monosulfated disaccharide homologues of ΔUA-GlcNS (Figure 9A), ΔUA2S-GlcN (Figure 9B), and ΔUA-GlcN6S (Figure 9C), the NH resonance of C38 can be seen to undergo the most significant upfield shift for the CTX A3−ΔUA-GlcNS sample compared to the one for CTX A3 by itself (Figure 9D). It suggests that the *N*-sulfate of GlcNS6S may be the crucial sulfate residue responsible for anchoring the heparin-derived disaccharide near position C38. It is also consistent with the suggestion that the GlcNS6S ring should point toward the core of the molecule as indirectly implied by the intermolecular NOE data.

NOE data for a mixture of the three monosulfated disaccharides, ΔUA-GlcNS, ΔUA2S-GlcN, and ΔUA-GlcN6S, were also used to determine the importance of the sulfation pattern when binding to CTX A3 (Figure 10). For the free form, all monosulfated oligosaccharides had similar negative NOE peaks (Figure 10A). However, the *N*-sulfated ΔUA-GlcNS had the strongest transfer NOE, indicating it bound more strongly to CTX A3 as seen from the change in the NOE signal from negative to positive for cross-peaks of $H3^b$ and $H4^b$ (Figure 10B). The important role of *N*-sulfate in the CTX−heparin interaction has previously been suggested by the binding study of *N*-desulfated high-molecular weight heparin (*5*). In contrast, 6-*O*-sulfate located on the same carbohydrate residue of ΔUA-GlcN6S produced no such effect. Interestingly, 2-*O*-sufate in the ΔUA2S ring appears to bind to CTX A3 strongly enough to allow the detection of a positive, although weaker, NOE. It suggests that 2-*O*-sulfate is also directly involved in the binding.

Molecular docking of the heparin-derived disaccharide onto CTX A3 was done by computer simulation taking into account all the available data. The average structure for the 50 ps molecular dynamic simulation is depicted as a ribbon diagram (Figure 11A) and an electrostatic surface model (Figure 11B). The average of the glycosidic angles was 60° ± 6° and −7° ± 8°, in accord with the CORCEMA result for the bound conformation (64° and −5°, respectively). CORCEMA calculations using the average coordinates of the complex gave an overall interresidue *R*-factor of 0.26, in accord with the results presented in Table 3. The electrostatic surface model of CTX A3 indicated that the heparin binding site is a cluster of positive charge with three lysine residues, and Leu6, Tyr22, and Cys38 are proximal to the binding site. The *N*-sulfate of GlcNS6S not only can bind to $NH_3^+\zeta$ of Lys12 but also can form hydrogen bonds with the NH of Cys38 and OH of the Tyr12 aromatic ring (Figure 11C). Lys35 interacts with the 6-*O*-sulfate through electrostatic interaction which leads to a rotation of the sulfate side chain from the *gt* to *gg* conformer to reduce the level of steric interactions. The 2-*O*-sulfate of the ΔUA2S ring interacts with $NH_3^+\zeta$ of Lys5 and forms a hydrogen bond with NH of Leu6. Otherwise, the ΔUA2S carboxyl group (COO^-) also interacts with the positive residue, Lys5, and contributes the same charge−charge interaction as 2-*O*-sulfate after the similar distances between the two negatively charged groups and $NH_3^+\zeta$ of Lys5 are considered. Since Lys5 is involved in the only obvious interaction between the ΔUA2S ring and CTX A3, the substitution of Lys5 for Gln5 in CTX Tγ would release ΔUA2S from interacting with the CTX molecule. As a result, CTX Tγ binding to heparin-derived disaccharide produces no conformational change in the glycosidic dihedral angle as compared to the free form.

DISCUSSION

The structure of the complex between CTX A3 and the heparin-derived disaccharide under nonaggregated conditions,

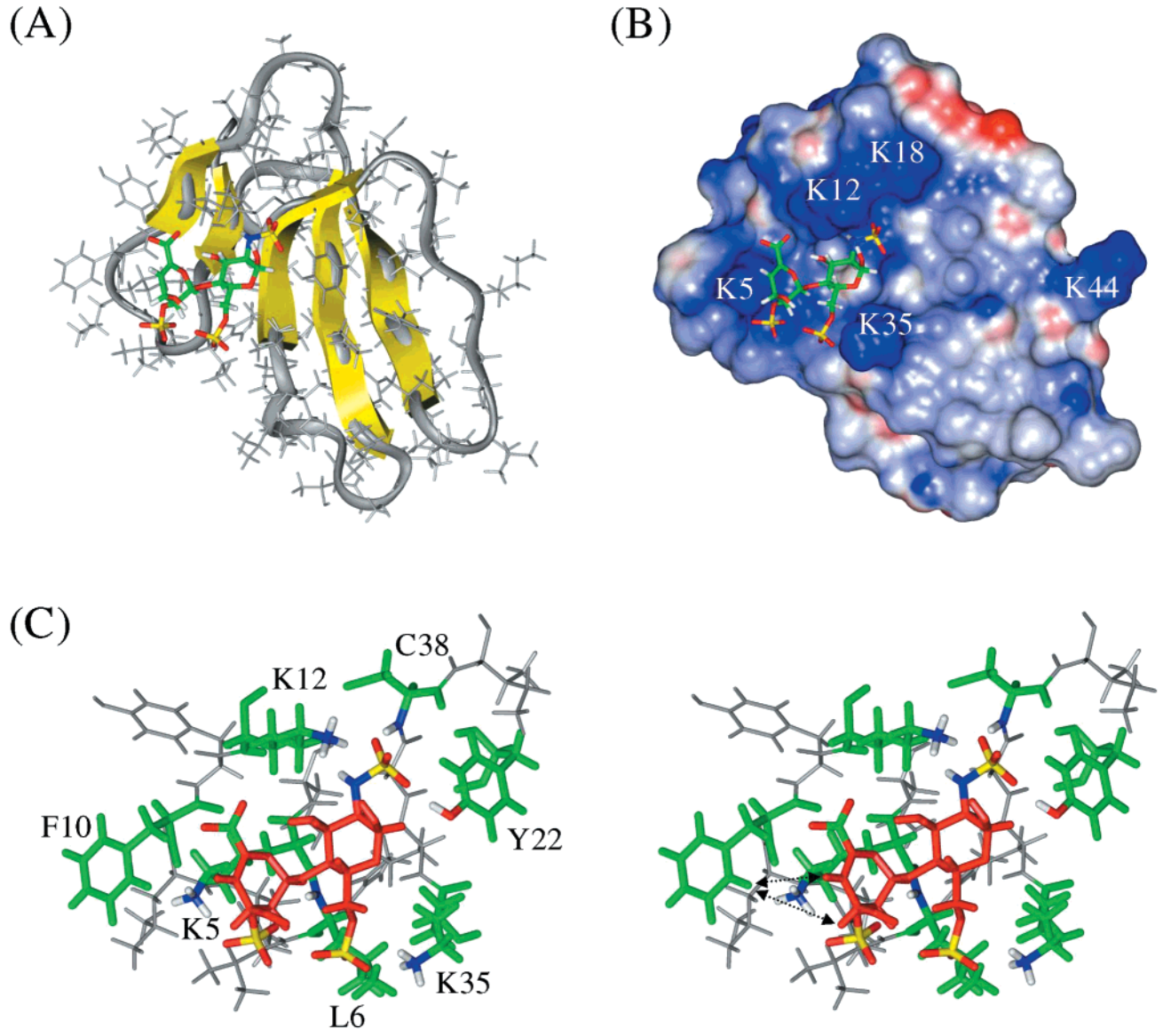

FIGURE 11: Molecular modeling diagrams of the CTX−heparin-derived disaccharide complex. (A) Overall structural view of the disaccharide bound to CTX A3, with a gray ribbon for the backbone and thick yellow ribbons for the five β-sheets. (B) Electrostatic surface of CTX A3 (blue for positive potential and red for negative potential) with disaccharide, where five positive residues located on the convex side are labeled. (C) Stereoview of a stick model of disaccharide with the neighboring protein residues. The intermolecular NOEs between 2,6H of F10 and $H3^b$ and $H4^b$ are indicated by arrows. The sugar is red, and the crucial protein residues are green. The charged groups involved in binding are colored according to the atom species (red, oxygen; green, carbon; blue, nitrogen; yellow, sulfate; and white, hydrogen). The structure presented here is the averaged structure from a 50 ps molecular dynamics calculation.

as depicted by the molecular docking of the bound conformation to the convex side of CTX, is consistent with NMR data, such as the chemical shift variation pattern of the protein, the transferred NOEs and *J* coupling constant for the sugar, and the intermolecular NOEs. For instance, the 6-*O*-sulfate orientation is found to adopt the *gg* conformer for the heparin disaccharide bound to CTX A3 as indicated by the *J* coupling constants of nearby protons of $H6_R^a/H5^a$ and $H6_S^a/H5^a$. This is mainly due to the steric hindrance arising from Lys35 protruding into the region. The observed weak intermolecular NOE between $H4^b$ of ΔUA2S and 2,-6H of Phe10 is consistent with the 6.4 ± 1.3 Å internuclear distance arising from the orientation of the disaccharide relative to CTX. The large chemical shift variation for the H_1^a and H_4^a protons in the GlcNS6S unit upon binding is reflective of their close protein contact in the complex.

The heparin-derived disaccharide binds to the convex side of CTX A3 by involving Lys12 and Lys5. The binding of CTX A3 to this disaccharide induced significant structural changes not only on the ring conformation of ΔUA2S but also on its glycosidic (Φ and Ψ) torsion angles. The disaccharide was also found to bind CTX Tγ, where Lys5 in CTX A3 has been replaced with Gln5 in CTX Tγ. However, the glycosidic linkage conformation of the bound form was the same as the one for the free form due to the lack of electrostatic interaction involving ΔUA2S. It should be emphasized that the Δ^4 unsaturated carbon bond of ΔUA2S produced by heparinase depolymerization does not affect the glycosidic angle of fully sulfated disaccharide of IdoA2S-GlcNS6S as judged by the similarity of their calculated (Φ and Ψ) energy maps (*38*). In addition, the difference in the orientations of carboxyl groups of ΔUA2S

and IdoA2S does not appear to perturb the interaction between disaccharide and CTXA3 since the carboxyl group of IdoA2S is also facing toward the protein surface to be able to interact with Lys5. It is likely that the structure of the disaccharide−CTX A3 complex with ΔUA2S-GlcNS6S should be applicable to that with IdoA2S-GlcNS6S.

The weaker binding of the disaccharide to CTX Tγ than to CTX A3 was also reflected in the kinetic parameters obtained from the analysis of the NOE buildup curves. CORCEMA analysis of the bound conformation further suggests that both k_{on} and k_{off} are ∼2 orders of magnitude greater for CTX Tγ than for CTX A3. This is consistent with the observation that the binding of heparin-derived disaccharide to CTX A3 induced a conformational change in the disaccharide, but binding to CTX Tγ produced little conformational change in the disaccharide. The comparable changes in the magnitudes of k_{on} and k_{off} explain how the weaker binding to CTX Tγ can give rise to a K_d value which is very similar to that of the stronger binding to CTX A3 (Table 3). Similar changes in both k_{on} and k_{off} for CTX Tγ relative to CTX A3 binding may be rationalized as follows. Binding to CTX Tγ is dominated by the GlcNS6S residue, while binding to CTX A3 involves both sugar residues. This process for CTX A3 is expected to be slower, especially if the binding of the second saccharide residue requires a conformational change. Conversely, dissociation of the CTX Tγ complex involves breaking of only GlcNS6S−protein contacts as compared to the involvement of two residues in the CTX A3 complex, a process which is again expected to be slower. From an energetic point of view, a 2 order of magnitude difference in terms of reaction rate would require an energy difference in the transition state of ∼2.7 kcal/mol. This is similar to the energy difference for the two conformations, A and B, shown in the energy contour map (Figure 7).

Lys12 is well conserved for all CTXs and has been shown to be able to bind to inorganic phosphate, which forms an additional hydrogen bond with OH of the Tyr22 and NH of Cys38 (*40*). The neighboring residues, forming a conserved hydrophobic cluster, were proposed to constitute a possible binding site for the phosphate group of lipids (*40*). The modification of a conserved residue (Lys12 or Tyr22) also leads to a dramatic decrease in lethal activity (*41*, *42*). Due to this observation, the peptide region responsible for lethality was concluded to be constituted by loop I and the base of loop II (*40*). The fact that the *N*-sulfate of the GlcNS6S residue interacts with CTX A3 at exactly the same site as the phosphate binding pocket is significant. When the similar size of the two inorganic ions is considered, it is reasonable to anticipate that they can form the same hydrogen bond network within this site. The neighboring residues that form a hydrophobic cluster might also serve as a common sulfate or phosphate binding site with molecules containing sulfate or phosphate groups.

This study has identified a novel binding site at the convex side of CTXs. This heparin binding site determined in a nonaggregated state is distinctly different from the binding site inferred from the comparative binding studies of 10 CTX homologues (*6*). It has also been suggested, based on the three-phase binding profiles detected by CD and absorbance, that two nonequivalent binding states of the CTX−heparin complex exist (*6*). One of the simplest explanations would be to assign them to the two nonequivalent binding sites located at the concave and convex sides of the CTX molecules. The absence of Lys5 on the convex side of the CTX Tγ molecule will necessarily decrease the heparin binding strength at this location as compared to that of CTX A3.

The presence of two heparin binding sites which have sequence-dependent affinities suggests that their interplay may constitute a regulatory function. One such hypothesis is that binding to the site on the convex side of the CTX would reverse the conformational change induced by the heparin binding at the concave side. This could explain the fact that CTX lacking Arg/Lys5 requires higher heparin concentrations to reverse the heparin-induced aggregation process. Indeed, we recently found that long chain heparin may produce conformational changes of CTX molecules in regions similar to those induced by the binding of phospholipid micelles (*43*). This novel observation also provides a simple explanation for how heparin binding to CTX may enhance the binding of CTX to phospholipid membranes.

Finally, in light of the possible binding specificity of different GAGs toward the binding site located at the convex side of CTX A3 (e.g., *N*-sulfate > 2-*O*-sulfate > 6-*O*-sulfate), it will be interesting to investigate how different binding specificities of GAGs for the two heparin binding sites may allow a delicate regulation of the heparin-induced aggregation process of GAG-binding proteins in general and CTX in particular.

REFERENCES

1. Dufton, M. J., and Hider, R. C. (1991) in *Snake Venom* (Harvey, A. L., Ed.) pp 259−272, Pergamon Press, New York.
2. Fletcher, J. E., and Jiang, M.-H. (1993) *Toxicon 31*, 669−695.
3. Lee, C. Y., Ed. (1979) *Snake Venom: Handbook of Experimental Pharmacology*, Vol. 52, Springer-Verlag, Berlin.
4. Patel, H. V., Vyas, A. A., Vyas, K. A., Liu, Y.-S., Chiang, C.-M., Chi, L.-M., and Wu, W. (1997) *J. Biol. Chem. 272*, 1484−1492.
5. Vyas, K. A., Patel, H. V., Vyas, A. A., and Wu, W. (1998) *Biochemistry 37*, 4527−4534.
6. Vyas, A. A., Pan, J.-J., Patel, H. V., Vyas, K. A., Chiang, C.-M., Sheu, Y.-C., Hwang, J.-K., and Wu, W. (1997) *J. Biol. Chem. 272*, 9661−9670.
7. Safran, M., Eisenstein, M., Aviezer, D., and Yayon, A. (2000) *Biochem. J. 345*, 107−113.
8. David, J. C., Venkataraman, G., Shriver, Z., Raj, P. A., and Sasisekharan, R. (1999) *Biochem. J. 341*, 613−620.
9. Waksman, G., and Herr, A. B. (1998) *Nat. Struct. Biol. 5*, 527−530.
10. Hoogewerf, A. J., Kuschert, G. S., Proudfoot, A. E., Borlat, F., Clark-Lewis, I., Power, C. A., and Wells, T. N. (1997) *Biochemistry 36*, 13570−13578.
11. Herr, A. B., Ornitz, D. M., Sasisekharan, R., Venkataraman, G., and Waksman, G. (1997) *J. Biol. Chem. 272*, 16382−16389.
12. Spivak-Kroizman, T., Lemmon, M. A., Dikic, I., Ladbury, J. E., Pinchasi, D., Huang, J., Jaye, M., Crumley, G., Schlessinger, J., and Lax, I. (1994) *Cell 79*, 1015−1024.
13. Lin, Y.-H., Lee, S.-C., Chang, P. Y., Rajan, P. K., Sue, S.-C., and Wu, W. (1999) *FEBS Lett. 453*, 395−399.
14. Venkataraman, G., Raman, R., Sasisekharan, V., and Sasisekharan, R. (1999) *Proc. Natl. Acad. Sci. U.S.A. 96*, 3658−3663.
15. Ogura, K., Nagata, K., Hatanaka, H., Habuchi, H., Kimata, K., Tate, S., Ravera, M. W., Jaye, M., Schlessinger, J., and Inagaki, F. (1999) *J. Biomol. NMR 13*, 11−24.

16. Schlessinger, J., Plotnikov, A. N., Ibrahimi, O. A., Eliseenkova, A. V., Yeh, B. K., Yayon, A., Linhardt, R. J., and Mohammadi, M. (2000) *Mol. Cell 6*, 743−750.
17. DiGabriele, A. D., Lax, I., Chen, D. I., Svahn, C. M., Jaye, M., Schlessinger, J., and Hendrickson, W. A. (1998) *Nature 393*, 812−817.
18. Rapraeger, A. C., Krufka, A., and Olwin, B. B. (1991) *Science 252*, 1705−1708.
19. Yamada, S., Murakami, T., Tsuda, H., Yoshida, K., and Sugahara, K. (1995) *J. Biol. Chem. 270*, 8696−8705.
20. Rice, K. G., Rottink, M. K., and Linhard, R. J. (1987) *Biochem. J. 244*, 515−522.
21. Chien, K.-Y., Chiang, C.-M., Hseu, Y.-C., Vyas, A. A., Rule, G. S., and Wu, W. (1994) *J. Biol. Chem. 269*, 14473−14483.
22. Bax, A., and Davis, D. G. (1985) *J. Magn. Reson. 65*, 355−360.
23. Piotto, M., Saudek, V., and Sklendar, V. (1992) *J. Biomol. NMR 2*, 661−665.
24. Uhrin, D., and Barlow, P. N. (1997) *J. Magn. Reson. 126*, 248−255.
25. Scheffler, K., Brisson, J.-R., Weisemann, R., Magnani, J. L., Wong, W.-T., Ernst, B., and Peters, T. (1997) *J. Biomol. NMR 9*, 423−436.
26. Uhrin, D., and Brisson, J.-R. (2000) *NMR in Microbiology: Theory and Applications*, pp 165−190, Horizon Scientific Press, Wymondham, U.K.
27. Kupce, E., and Freeman, R. (1995) *J. Magn. Reson., Ser. A 112*, 134−137.
28. Moseley, H. N. B., Curto, E. V., and Krishna, N. R. (1995) *J. Magn. Reson., Ser. B 108*, 243−261.
29. Krishna, N. R., and Moseley, H. N. B. (1999) in *Biological Magnetic Resonance*, Vol. 17, pp 223−307, Kluwer Academic/Plenum Publishers, New York.
30. Krishna, N. R., Agresti, D. G., Glickson, J. D., and Walter, R. (1978) *Biophys. J. 24*, 791−814.
31. Xu, Y., Krishna, N. R., and Sugar, I. P. (1995) *J. Magn. Reson., Ser. B 107*, 201−109.
32. Homans, S. W. (1990) *Biochemistry 29*, 9110−9118.
33. Huige, C. J. M., and Altona, C. (1995) *J. Comput. Chem. 16*, 56−79.
34. Hricovini, M., Guerrini, M., and Bisio, A. (1999) *Eur. J. Biochem. 261*, 789−801.
35. Ragazzi, M., Ferro, D. R., Provasoli, A., Pumilia, P., Cassinari, A., Torri, G., Guerrini, M., Casu, B., Nader, H. B., and Dietrich, C. P. (1993) *J. Carbohydr. Chem. 12*, 523−535.
36. Mulloy, B., Forster, M. J., Jones, C., and Davies, D. B. (1993) *Biochem. J. 318*, 93−102.
37. Sue, S.-C., Jarrell, H. C., Brisson, J.-R, and Wu, W. (2001) *Biochemistry* (submitted for publication).
38. Mikhailov, D., Linhard, R. J., and Mayo, K. H. (1997) *Biochem. J. 328*, 51−61.
39. Rees, B., Bilwes, J., Samama, P., and Moras, D. (1990) *J. Mol. Biol. 214*, 281−297.
40. Gilquin, B., Roumestand, C., Zinn-Justin, S., Menez, A., and Toma, F. (1993) *Biopolymers 33*, 1659−1675.
41. Gatineau, E., Toma, F., Montenay-Garestier, T., Takechi, M., Fromageot, P., and Menez, A. (1987) *Biochemistry 26*, 8046−8055.
42. Gatineau, E., Takechi, T., Bouet, F., Mansuelle, P., Rochat, H., Harvey, A. L., Montenay-Garestier, T., and Menez, A. (1990) *Biochemistry 29*, 6480−6489.
43. Sue, S.-C., Chien, K.-Y., Huang, W.-N., Joseph, K. A., Chen, K.-M., and Wu, W. (2001) *J. Biol. Chem.* (submitted for publication).

BI010847N